Title

Genomic and Transcriptomic Analysis Reveals Incremental Disruption of Key Signaling Pathways during Melanoma Evolution

Journal

Cancer Cell, 34(1)

ISSN

1535-6108

Authors

Shain, A Hunter
Joseph, Nancy M
Yu, Richard
et al.

Publication Date

2018-07-01

DOI

10.1016/j.ccell.2018.06.005

Peer reviewed

HHS Public Access

Author manuscript

Cancer Cell. Author manuscript; available in PMC 2019 January 04.

Published in final edited form as:

Cancer Cell. 2018 July 09; 34(1): 45–55.e4. doi:10.1016/j.ccell.2018.06.005.

Genomic and Transcriptomic Analysis Reveals Incremental Disruption of Key Signaling Pathways during Melanoma Evolution

A. Hunter Shain[1,2,6,*], **Nancy M. Joseph**[3], **Richard Yu**[1,2], **Jamal Benhamida**[3], **Shanshan Liu**[1,2], **Tarl Prow**[4], **Beth Ruben**[1,3,5], **Jeffrey North**[1,3], **Laura Pincus**[1,3], **Iwei Yeh**[1,2,3], **Robert Judson**[1,2], and **Boris C. Bastian**[1,2,3,*]

[1]University of California San Francisco, Department of Dermatology, San Francisco, CA, USA

[2]University of California San Francisco, Helen Diller Comprehensive Cancer Center, San Francisco, CA, USA

[3]University of California San Francisco, Department of Pathology, San Francisco, CA, USA

[4]Future Industries Institute, University of South Australia, Adelaide, SA, Australia

[5]Palo Alto Medical Foundation, Palo Alto, CA, USA

[6]Lead Contact

SUMMARY

We elucidated genomic and transcriptomic changes that accompany the evolution of melanoma from premalignant lesions by sequencing DNA and RNA from primary melanomas and their adjacent precursors, as well as matched primary tumors and regional metastases. In total, we analyzed 230 histopathologically distinct areas of melanocytic neoplasia from 82 patients. Somatic alterations sequentially induced mitogen-activated protein kinase (MAPK) pathway activation, upregulation of telomerase, modulation of the chromatin landscape, G1/S checkpoint override, ramp-up of MAPK signaling, disruption of the p53 pathway, and activation of the PI3K pathway; no mutations were specifically associated with metastatic progression, as these pathways were perturbed during the evolution of primary melanomas. UV radiation-induced point mutations steadily increased until melanoma invasion, at which point copy-number alterations also became prevalent.

*Correspondence: alan.shain@ucsf.edu (A.H.S.), boris.bastian@ucsf.edu (B.C.B.).

AUTHOR CONTRIBUTIONS

A.H.S. and B.C.B. supervised the study. A.H.S., N.M.J., R.J., and B.C.B. designed the study. B.C.B. and T.P. provided archival tissues used in this study. A.H.S. and R.Y. performed genotyping. A.H.S. and B.C.B. analyzed genotyping results. N.M.J. developed RNA-seq protocols used in the study. N.M.J., R.J., J.B., and A.H.S. performed microdissections. S.L. prepared next-generation sequencing libraries. B.R., J.N., L.P., I.Y., and B.C.B. performed histopathological evaluations. A.H.S. and B.C.B. wrote the paper. All authors reviewed the manuscript.

DECLARATION OF INTERESTS

B.C.B. is a consultant for Lilly Inc.

SUPPLEMENTAL INFORMATION

Supplemental Information includes seven figures and five tables and can be found with this article online at https://doi.org/10.1016/j.ccell.2018.06.005.

In Brief

Shain et al. show sequential MAPK pathway activation, telomerase upregulation, chromatin landscape modulation, G1/S checkpoint override, MAPK signaling ramp-up, p53 pathway disruption, and PI3K pathway activation during the evolution from pre-malignant lesions to melanoma, but no metastasis-specific mutations.

Graphical Abstract

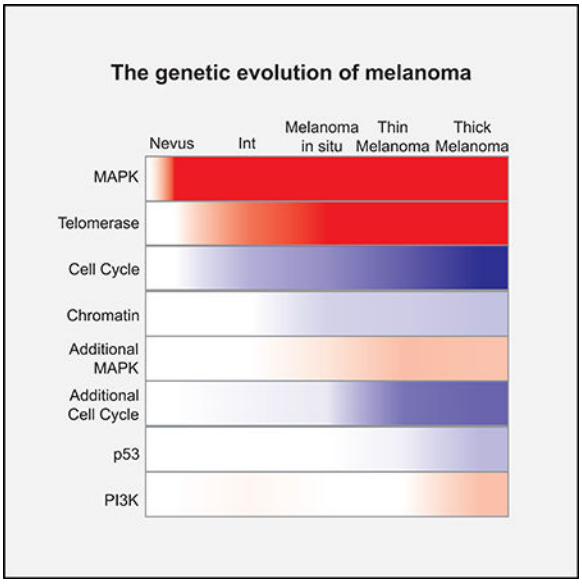

INTRODUCTION

Melanocytic neoplasms range from benign lesions called melanocytic nevi to malignant lesions termed melanomas. Melanomas can metastasize at an early stage and the risk of death increases with the thickness of the primary tumor. While the somatic mutations and expression profiles of melanoma metastases and some advanced primary tumors have been cataloged (Cancer Genome Atlas Network, 2015), the molecular events during the early phases of melanoma evolution remain incompletely understood (Shain and Bastian, 2016). Characterizing the molecular alterations that drive melanoma evolution and progression could reveal biomarkers that assist in diagnosis and staging of patients and reveal critical barriers to transformation that become overrun during melanoma evolution.

We recently began to delineate the sequential order in which pathogenic mutations undergo selection during melanoma evolution by sequencing melanomas and their adjacent, intact precursor lesions (Shain et al., 2015a). However, that study was restricted to analyses of DNA and limited in sample size, precluding the establishment of the sequential order in which many critical mutations undergo selection. Here we extend this investigation to identify changes that accompany specific evolutionary stages during melanoma progression.

RESULTS

We performed targeted sequencing of several hundred common cancer genes (Table S1) on 230 histopathologically distinct areas of melanocytic neoplasia, microdissected from 82 patients' tumors (Figures S1A–S1C; Table S2)—48 patients' tumors were newly sequenced and the remainder were reanalyzed from our prior work (Shain et al., 2015a). Matched RNA sequencing (RNA-seq) was performed on 42 areas representing different progression stages from 20 of these patients. The genetic evolution of each individual melanoma is detailed in our Mendeley Dataset (https://doi.org/10.17632/nrywwbx6fm.2). Here, we investigated the representative patterns in which genetic alterations arose during progression.

MAPK Signaling Amplifies during Melanoma Progression

Mutations predicted to activate the mitogen-activated protein kinase (MAPK) pathway were identified in all patients' tumor areas, irrespective of their progression stage (Figures 1A and S2A), suggesting that constitutive MAPK pathway activation is necessary for a melanocytic neoplasm to establish. The two most common mutations in this pathway, $BRAF^{V600E}$ and $NRAS^{Q61(K/L/R)}$, are known to occur in a mutually exclusive pattern in melanoma; however, multiple mutations in the MAPK pathway can be found in individual tumors. For example *NF1*, *MAP2K1*, or weakly activating *BRAF* mutations are commonly found together with alterations elsewhere in the MAPK signaling cascade in the same tumor (Cancer Genome Atlas Network, 2015; Krauthammer et al., 2015; Shain et al., 2015b). As another example, mutated genes in the MAPK pathway in melanoma can also be subjected to copy-number gains or allelic imbalance, increasing the absolute or relative gene dosage of the oncogenic alleles (Maldonado et al., 2003). We noted that the number of mutations per sample in genes known to activate the MAPK pathway increased along with the progression from pre-malignant lesions to melanoma (Figure 1A, green bars with the specific combination of alterations iterated to the right; Figures S2B and S2C). We categorized mutations into strongly and weakly activating mutations based on published functional data (see the STAR Methods), and noted that combinations of MAPK pathway mutations inferred to result in strong pathway activation were confined to later progression stages (Figure 1A, striped green bars).

To corroborate that the intensity of MAPK signaling is ramped up during progression, we assessed the expression levels of mutant and wild-type alleles of oncogenes in the MAPK pathway. The relative expression of mutant *BRAF*, *NRAS*, and *MAP2K1* transcripts correlated with the neoplastic cell content of the sample, as expected (Figure 1B); however, after accounting for this trend, melanomas consistently expressed proportionally higher levels of mutant transcripts than nevi (Figures 1B and 1C). Elevated expression of mutant oncogene transcripts was often found in samples with copy-number increases of the mutant allele, but even melanomas without such additional genetic alterations at the locus of the oncogene also showed this pattern (Figure 1C), possibly indicating preferential transcription of the mutant allele. We also inferred the activity of MAPK activation in each neoplasm by measuring the intensity of an MAPK transcriptional signature (Joseph et al., 2010). The intensity of the signature correlated with progression stage and the number of MAPK-

pathway-activating alterations, corroborating the ramp-up of pathway activation, as suggested by the pattern of somatic mutations (Figures 1D and S2D).

In aggregate, both the genetic and transcriptomic data indicate that MAPK signaling becomes activated at the earliest stage of neoplasia but progressively ramps up as malignant transformation proceeds.

Telomerase Is Expressed Early during Progression

While absent in nevi, *TERT* promoter mutations became evident in most intermediate neoplasms and were present in nearly all melanomas, irrespective of their tumor thickness (Figure 2A). *TERT* alterations typically succeeded MAPK-pathway-activating mutations (Figure S3A), but preceded other progression-associated mutations (Figure S3B). In the samples with available RNA-seq data, *TERT* expression was significantly elevated in samples harboring promoter mutations (Figure 2B)—this was intriguing because the melanoma study by The Cancer Genome Atlas noted only a modest increase in *TERT* expression when they compared melanomas with and without *TERT* promoter mutations (Cancer Genome Atlas Network, 2015). Our comparison was different in that we compared pre-malignant lesions without promoter mutations to the melanomas they formed and which had acquired promoter mutations during this transformation. This analysis revealed an unequivocal rise in telomerase expression in tumor areas with promoter mutations compared with their respective pre-malignant lesions that did not harbor *TERT* promoter mutations.

The Chromatin-Remodeling Landscape Shifts at the Transition to Melanoma

The human switch/sucrose non-fermentable (SWI/SNF) chromatin remodeling complex, commonly abbreviated SWI/SNF, is composed of approximately 15 distinct subunits encoded by different genes, which act as tumor suppressors in a broad range of cancers (Shain and Pollack, 2013). In melanoma, inactivating mutations preferentially affect *ARID2* and, to a lesser extent, *ARID1A*, *ARID1B*, *PBRM1*, and *SMARCA4* (Cancer Genome Atlas Network, 2015; Hodis et al., 2012). The SWI/SNF complex antagonizes polycomb repressive complex 2 (PRC2), which silences gene expression by tri-methylation of lysine 27 on histone H3, to modulate expression of target genes (Wilson et al., 2010). In melanoma, activation of PRC2 can also occur via gain-of-function *EZH2* mutations, the enzymatic subunit of PRC2 (Cancer Genome Atlas Network, 2015).

Somatic alterations that inactivate SWI/SNF or activate PRC2 became evident at the melanoma *in situ* progression stage and increase in frequency during later stages (Figure 3A). In several particularly informative cases, the emergence of these mutations could be pinpointed precisely to the transition to the melanoma state (Figure S4). These genetic findings indicate that the balance of chromatin-remodeling activity shifts in favor of PRC2 over SWI/SNF when pre-malignant lesions progress to melanoma.

Unsupervised hierarchical clustering of the RNA-seq data from areas of different progression stages also supported this shift, revealing a differentially expressed cluster of genes heavily enriched for PRC2 targets and downregulated in malignant lesions (Figures 3B, S5A, and S5B). This expression pattern is thus consistent with the increased frequency of mutations disabling SWI/SNF complexes or activating PRC2 complexes during

progression (Figure 3C). Notably, melanomas without mutations in chromatin remodeling genes also showed this expression signature. Our methods of classifying chromatin remodeling aberrations as pathogenic were conservative and took into account the overall high mutation burden with numerous passenger mutations in melanomas, which may have led us to inadvertently under-call the mutation frequency in chromatin remodelers (see the STAR Methods). It is also possible that the balance of chromatin remodeling activity is affected by mechanisms other than mutations affecting the SWI/SNF or PRC2 genes covered by our assay. In summary, both genetic and transcriptomic data suggest that PRC2 reshapes the chromatin and expression landscape at the transition to melanoma.

Impaired Cell-Cycle Regulation at the Transition to Invasive Melanoma

Somatic alterations known to disrupt genes involved in the G1/S cell-cycle checkpoint emerged in intermediate progression stages and incrementally increased in frequency in subsequent progression stages (Figures 4A and S6A–S6C). While the somatic alterations in intermediate and melanoma *in situ* stages were typically heterozygous and spared one allele, invasive melanomas commonly had biallelic inactivation of critical cell-cycle checkpoint genes or combinations of somatic alterations affecting different genes involved in checkpoint function (Figure 4A, green bars).

The most common somatic alterations affected the *CDKN2A* gene, which encodes two protein products, $p16^{INK4A}$ and $p14^{ARF}$, operating in the Rb and p53 pathways, respectively (Sharpless and Chin, 2003). We distinguished their individual transcripts using reads containing transcript-specific splice junctions (Figures 4B and 4C). For samples with somatic point mutations, we determined the proportion of reads mapping to the mutant or wild-type transcripts (Figures 4B and 4C, striped versus solid bars). We inferred the relative transcriptional contributions from stromal cells using information from the eight samples harboring homozygous deletions of *CDKN2A* or hemizygous mutations affecting *CDKN2A*, reasoning that in these samples any transcripts of wild-type $p16^{INK4A}$ or $p14^{ARF}$ would be derived from stromal cells. The highest stromal expression of $p16^{INK4A}$ or $p14^{ARF}$ found in these eight samples is indicated by the dotted lines in Figures 4B and 4C, suggesting that stromal cells only minimally contribute to the overall abundance of these transcripts in tumor samples.

There is a longstanding debate as to the relative importance of $p16^{INK4A}$ and $p14^{ARF}$ (Sharpless and Chin, 2003) during melanoma progression, and our data implicate $p16^{INK4A}$ as the predominant tumor suppressor acting at the transition to invasive melanoma. This is because $p16^{INK4A}$ expression was significantly decreased in melanomas compared with nevi ($p = 1.1 \times 10^{4}$, Wilcoxon rank-sum test), whereas there was no significant difference for $p14^{ARF}$ expression levels (Figures 4B, 4C, S6D, and S6E). For most melanomas, decreased $p16^{INK4A}$ expression occurred even in the absence of genetic alterations affecting both alleles of *CDKN2A*, suggesting that other factors such as epigenetic alterations can contribute to the suppression of $p16^{INK4A}$. There was a small subset of melanomas for which $p16^{INK4A}$ expression was relatively high, and these melanomas tended to harbor mutations in other cell-cycle checkpoint genes downstream of $p16^{INK4A}$ (Figure 4B). In

aggregate, the genetic and transcriptomic data indicate disruption of the G1/S checkpoint at the transition to invasive melanoma.

The Evolution of Advanced Primary Melanomas and Regional Metastases

Invasive melanomas can be stratified by the thickness of the primary tumor, which is correlated with prognosis (Balch et al., 2009). Mutations in genes operating in the p53 or phosphatidylinositol 3-kinase (PI3K) pathways were each found in approximately 25% of thick melanomas (i.e., invasive melanomas with a tumor thickness exceeding 1 mm), but were rare in earlier stages of melanoma progression, suggesting that that these mutations undergo positive selection later during the progression cascade (Figures 5A–5D). We did not note other differences between thin and thick primary melanomas.

Our cohort included 12 primary melanomas from which the matching regional metastases were also analyzed. We sought to identify whether any specific pathogenic mutations could be associated with the transition to metastatic disease. Most of the pathogenic mutations were shared between primary tumors and metastases, placing them on the trunk of their respective phylogenetic trees (Figure S7). By contrast, five of the metastases and seven of the primary melanomas each had private pathogenic mutations (Figure S7), placing them on branches of their respective trees. The most recurrent branchial mutations were inactivating mutations of *PTEN* and genetic alterations that resulted in increased gene dosage of oncogenic MAPK mutations; however, these mutations were equally distributed over the branches of primary melanomas and metastases, indicating that their selection was not specifically associated with metastatic spread to regional lymph nodes. Overall our study did not yield any mutations that were specifically associated with primary tumors or regional metastases.

The Mutagenic Forces that Shape Melanomas throughout their Evolution

The types of mutations that accumulate during melanoma progression can illuminate the mutational processes operating at various phases of progression. The point mutation burden in melanoma *in situ* was ten mutations per megabase, and this mutational burden only marginally increased in invasive melanomas (Figure 6A). This finding indicates that most point mutations accumulate before melanomas become invasive, consistent with the notion that UV radiation is the dominant mutagen but, likely due to its limited cutaneous penetration, contributes less to the mutagenesis of invasive melanoma cells. In contrast, the fraction of the genome affected by copy-number alterations (CNAs) increased significantly at the transition to invasive melanoma and thereafter (Figure 6B). Furthermore, CNAs had a strong tendency to affect certain chromosomal regions in a stereotypic sequential order (Figure 6C).

Our study included advanced primary melanomas or metastases that evolved from four types of precursor lesions—nevi, intermediate neoplasms, *in situ* melanomas, and invasive melanomas. We constructed phylogenetic trees that were representative of these four progression trajectories by calculating the median trunk and branch lengths from all the individual trees corresponding to each of these four progression routes (Figure 6D).

For the most part, nevi did not possess any private mutations, reflected by the absence of a branch emerging from the precursor node in the first tree of Figure 6D. This observation indicates that neoplastic cells within nevi are likely the result of a single dominant wave of clonal expansion. By contrast, intermediate neoplasms and melanomas *in situ* did contain private mutations, as indicated by the short branches emanating from the precursor nodes in the second and third trees. Invasive melanomas and their matched metastases shared the majority of their somatic alterations—i.e., point mutations and copy-number changes—resulting in a proportionally longer trunk (fourth three of Figure 6D).

When we compared the mutational signatures between mutations situated on the trunks and branches of the different progression trajectories, we found that UV radiation-induced mutations were ubiquitous at every evolutionary time point (Figure 6D, lower panel). The predominance of UV signature mutations in the private mutations of metastases, which are not exposed to UV radiation, indicates that these mutations likely arose in a UV radiation-exposed subclone of the primary melanoma that subsequently spawned the metastasis.

DISCUSSION

In a simple model of tumor progression, a series of binary events activate or inactivate critical signaling pathways in a sequence that leads to a fully transformed state. Our analysis of DNA and RNA from melanocytic neoplasms, spanning multiple evolutionary stages of the same neoplastic process, reveals a more complicated pattern, in which pathways are incrementally perturbed by multiple, independent genetic alterations. For example, nevi typically showed only a single activating mutation in the MAPK pathway, but melanomas, particularly in the advanced stages, typically had multiple such alterations (Figure 7). This may indicate that high levels of MAPK signaling are not tolerated and/or do not confer an advantage to nevus cells before additional pathways are disrupted. Combinations of multiple activating mutations in the MAPK pathway have been described in melanomas that become resistant to targeted therapy (Shi et al., 2014), but our data indicate that they already arise and undergo positive selection during the natural evolution of primary melanomas. It remains to be determined whether the multiple activating mutations are a requirement for the melanoma state, or whether they simply represent a positive selection of cells with a higher proliferation rate, while equally transformed malignant cells with only singular pathway alterations remain present in the background. A scenario in which multiple subclones with different genetic states of pathway activation coexist is daunting from a therapeutic perspective, as it facilitates outgrowth of those clones that can maintain pathway activation in the presence of inhibitory drugs.

A similar pattern of incremental independent “hits” on the same pathway was observed in tumor suppressor pathways. Intermediate melanocytic neoplasms and melanomas *in situ* often had mono-allelic mutations of genes involved in cellcycle checkpoints, suggesting that these genes are haploinsufficient, in that loss of a single allele already confers some selective advantage. In contrast, the phenotype of invasive melanoma was associated with multiple aberrations, typically biallelic inactivation of *CDKN2A*. Functional data corroborate this association, as *CDKN2A* deletions, engineered into primary human melanocytes, confer

migratory, invasive, and metastatic phenotypes (Zeng et al., 2018 [this issue of *Cancer Cell*]).

A feature distinguishing benign and malignant melanocytic neoplasms arose from our genomic and transcriptomic analyses. Mutations in SWI/SNF chromatin remodeling genes emerged at the transition to melanoma, thereby shifting the balance of chromatin remodeling activity in favor of PRC2. Our genetic and transcriptomic observations are concordant with published functional data, as it has been shown that ablation of *EZH2*, which encodes the enzymatic subunit of PRC2, has no discernible effect on normal melanocyte biology or nevus melanocyte biology, yet *EZH2* is essential for the maintenance of the melanoma state (Zingg et al., 2015). In addition, EZH2 is upregulated in the presence of immune infiltration, and its expression in melanoma cells silences immunogenicity and antigen presentation (Zingg et al., 2017). These findings may explain the high activity of EZH2 in melanomas without SWI/SNF mutations, and they further underscore the critical role of PRC2 in driving melanoma.

Our study also shows that certain alterations in advanced melanomas appear comparatively later during melanoma progression. Somatic alterations affecting the p53 and PI3K pathways were more prevalent in thick melanomas (invasive melanomas of tumor thickness over 1 mm) and also enriched in the terminal branches of phylogenetic trees. These observations suggest that in melanoma these alterations do not confer a selective advantage until several other pathways have been perturbed, and may explain why germline variants that disrupt these signaling pathways confer little to no increased risk of melanoma (Kleihues et al., 1997; Tan et al., 2012).

While some primary melanomas and matching regional metastases did have pathogenic mutations in only one of the compartments, there were no mutations exclusively found in metastases across cases. Other studies that have profiled primary melanomas and their matched metastases have also failed to identify recurrent mutations specific to the metastatic areas (Ding et al., 2014; Gartner et al., 2012; Sanborn et al., 2015; Shain and Bastian, 2016). These observations suggest that primary melanomas and metastases tend to select for the same set of pathogenic mutations.

In addition to the findings reported here, we also reproduced the salient findings from earlier studies of melanoma progression (Shain and Bastian, 2016; Shain et al., 2015a). In particular, we confirmed that *TERT* expression as a consequence of promoter mutations arises in early stages of melanocytic neoplasia, and we further demonstrate here that this coincides with upregulation of *TERT* expression. We also confirm that different subtypes of melanoma evolve in distinct trajectories.

In conclusion, our study offers insights into the genetic alterations and their transcriptional consequences as melanomas evolve from pre-malignant lesions. The data reveals candidate biomarkers to be validated for clinical utility in staging of melanocytic neoplasms and also illuminates the barriers to transformation that become disrupted during melanoma progression.

STAR⋆METHODS

CONTACT FOR REAGENT AND RESOURCE SHARING

Further information and requests for resources and reagents should be directed to and will be fulfilled by the lead contact, Hunter Shain (Alan.Shain@ucsf.edu).

EXPERIMENTAL MODEL AND SUBJECT DETAILS

We selected melanocytic neoplasms from 82 patients. Two cases were from the Dermatology Research Centre in Queensland Australia and the remaining were from the UCSF Dermatopathology Archive. In total, we sequenced 230 histopathologically distinct areas from these patients' tumors. The histopathologic spectrum of all areas is shown in Figure S1 and described in Table S2. Briefly, from 52 patients, biopsies included intact precursor and descendent areas that could be clearly separated by microdissection. We also sequenced matched primary and metastatic melanomas (all regional metastases) from 12 patients. Finally, we sequenced standalone lesions from 18 patients. 45 cases were newly sequenced, and 37 cases were previously sequenced (Shain et al., 2015a) and reanalyzed here. This study was approved by the UCSF human research protection program, and all tissues were collected in accordance with the institutional review board with regard to informed consent.

METHOD DETAILS

Histopathologic Evaluation—Histopathologic areas from each tumor were independently evaluated by a panel of 5–8 dermatopathologists. The median and interquartile range of assessments are indicated in Figure S1 and Table S2. For comparisons across patients' tumors, microdissected areas were grouped into the following categories based on the extent of their progression: nevi, intermediate lesions, melanomas *in situ*, thin invasive melanomas, thick invasive melanomas, and metastatic melanomas. In several instances, disagreement in staging arose between benign and intermediate areas. When the median assessment was 'benign' but the interquartile range extended into the intermediate category, areas were classified into the intermediate category. Invasive melanomas less than 1 mm in thickness (Stage T1 disease) were categorized as 'thin invasive' and melanomas greater than 1 mm in thickness (Stage T2+ disease) were categorized as 'thick invasive'.

Microdissection—Tissues were microdissected with a scalpel under a dissection microscope from 10 μm unstained FFPE sections. Dissections were supervised by a pathologist with the intent to maximize neoplastic cell content (i.e., limit stromal cell contamination). For cases in which matched RNA-seq was also performed, every other level was utilized for RNA-seq. Genomic DNA was isolated using the Qiagen DNA FFPE Tissue Kit (p/n 56404). Total RNA was isolated using the Agencourt FormaPura Kit (A33341).

Inferring MAPK Activity from Transcriptional Profiles—Phospho-ERK is commonly used to measure MAPK activity for *in vitro* studies, but it is a not a good marker for *in situ* studies of melanoma (Houben et al., 2008). Therefore, we estimated MAPK signaling activity in each neoplasm from the intensity of a MAPK expression signature, as previously defined (Joseph et al., 2010). In Figure S2D, the samples (columns) are rank-ordered by the strength of their MAPK gene expression signature. The gene expression

levels for each gene known to be downregulated upon MAPK-pathway stimulation were multiplied by negative one and then averaged with gene expression levels of each known known to be upregulated upon MAPK-pathway stimulation (Figure S2D) – this produced a single value for each sample that attempts to capture the strength of pathway activation (Figures S2D and 1D).

Classifying 'Strong' and 'Weak' MAPK Mutations—We differentiate between 'weak' and 'strong' MAPK-activating mutations, as indicated in Table S3 (also listed on the right portion of Figure 1A). To define the strength of each mutation, we first consulted studies that directly compare the activities of these mutations (Krauthammer et al., 2015; Monsel et al., 2010; Nikolaev et al., 2012; Wan et al., 2004), and we defined a mutation as strongly activating if its activity is comparable to levels of $BRAF^{V600E}$ or $NRAS^{Q61(R/K/L)}$.

Unfortunately, not every mutation has been functionally characterized, but many are instead known to occur in patients with RASopathy syndromes, a set of phenotypically overlapping syndromes caused by germline alterations known to activate the MAPK pathway. We reasoned that these are likely to be weakly-activating mutations because they are found in the germline and therefore are tolerated during development into adulthood. Notably, the activity of some RASopathy mutations has been also investigated, confirming that they are comparatively weak in their activity (Krauthammer et al., 2015; Wan et al., 2004).

Finally, we scrutinized the remaining mutations that could not be classified by either of these criteria and grouped them as follows. (Overall, these mutations occurred in a small number of samples, and our conclusions would not be influenced if they were removed from the analysis.) The $GNA11^{R183C}$ mutation is an uncommon hotspot mutation thought to be weaker than mutations affecting codon 209 of *GNA11* (Van Raamsdonk et al., 2010) – though the $GNA11^{R183C}$ mutation has not been directly compared to *BRAF* or *NRAS* mutations, we reason that it is likely to be a weak activator of MAPK signaling. We classified the $KRAS^{Q61R}$ mutation as strongly activating because of its similarity to *NRAS* codon 61 mutations. We categorized the *RAF1* fusion as strongly activating because of its similarity to *BRAF* fusions, which are thought to be comparable to $BRAF^{V600E}$ in their signaling strength (Botton et al., 2013). The $MAP2K1^{IK103del}$ and $MAP2K1^{K57E}$ mutations have not been functionally investigated, but the more common *MAP2K1* codon 124 mutations have been shown to be weakly activating (Nikolaev et al., 2012); therefore, we classify these other *MAP2K1* mutations as also being weakly activating. The *CCND1* and *RAF1* amplifications only affected wild-type copies of those genes, and thus we classified these alterations as weakly activating.

Classifying Pathogenic Chromatin Remodeling Mutations—In Figure 3, we report the frequency of pathogenic SWI/SNF and PRC2 mutations at each phase of melanoma progression. These two chromatin remodeling complexes are composed of nearly thirty subunits encoded by genes with a considerable genomic footprint. Considering the high mutation burden of cutaneous melanoma, we elected to only consider those mutations that are bona fide pathogenic alterations to avoid overcalling spurious mutations reflecting the high background mutation rate. For PRC2, we considered *EZH2* hotspot mutations affecting codon 641 as pathogenic. *EZH2* is the catalytic subunit of PRC2 responsible for histone H3

lysine 27 methylation, and these mutations have been functionally characterized to confer gain-of-function to the complex. For SWI/SNF, we considered any mutation affecting *ARID2* and truncating mutations affecting *SMARCA4*, *ARID1A*, *ARID1B*, and *PBRM1* as pathogenic. These five subunits are the main mutational nodes affecting SWI/SNF across all cancers (Shain and Pollack, 2013). In melanoma, *ARID2* is a bona fide tumor suppressor, because it harbors a high frequency of mutations heavily skewed towards loss-of-function mutations (Hodis et al., 2012; Krauthammer et al., 2012). The mutation burdens of *SMARCA4*, *ARID1A*, *ARID1B*, and *PBRM1* are also skewed towards loss-of-function mutations, albeit to a lesser degree, and for this reason, we only considered truncating mutations affecting these genes in our study. SWI/SNF genes are frequently contained in regions affected by large deletions in melanoma, but to avoid overcalling of genetic alterations, we only considered deletions that were focal (only a single case had a focal homozygous *ARID1B* deletion).

Assessing Point Mutation and Copy Number Burdens—The fraction of the genome affected by copy number changes was determined from the segmented copy number data (Table S4). Two criteria were used in order to filter out segmentation artifacts (false positives) and subclonal copy number alterations. First, we required that the segment be supported by 25 or more probes. Second, the amplitude of the copy number alteration was required to exceed a threshold of 75% of the theoretical value for a single copy gain or loss in a pure sample with a fully clonal copy number change, which was specifically determined for each tumor area based on the proportion of neoplastic cells in that tumor area. The point mutation burden of each tumor area was calculated from the number of single-nucleotide somatic mutations and the genomic footprint sequenced. To supplement the numbers of thick melanomas and metastatic melanomas, we also include the point mutation burdens and copy number burdens from TCGA melanoma cases (Cancer Genome Atlas Network, 2015).

QUANTIFICATION AND STATISTICAL ANALYSES

DNA-seq and Analysis—Due to the small size of some of the tumor areas and formalin fixation of every tumor, many samples had low library complexity, as would be expected (Hedegaard et al., 2014; Kerick et al., 2011; Palescandolo et al., 2012). The primary goal of our study was to pinpoint the emergence of known pathogenic alterations during the evolution of melanoma, so we elected to perform targeted sequencing (Table S1 for baits) in order to ensure high sequencing coverage (average of 271X).

Two panels of baits were used – the first batch of cases was sequenced on a 293-gene panel, and the second batch of cases was sequenced on a 538-gene panel. The specific genes on each panel are indicated in Table S1. Both panels contain established melanoma genes. The latter panel includes many additional genes, involved in other cancers, but none of them were implicated as driver genes during the course of melanoma progression in this study. This finding supports our decision to sequence more samples at higher coverage, increasing the sensitivity of detection, rather than fewer samples with a larger gene panel (e.g. whole exome). The high sequencing coverage allowed us to identify genetic alterations, even in the presence of stromal cells, which contributed to 10–90% (median 45%) of sequencing reads.

The tradeoff for using a panel of fewer genes is that the reduced footprint tends to yield too few somatic mutations per sample, hampering the analysis of mutational signatures. We addressed this by performing mutational signature analyses on aggregated mutational data from similar samples (Figure 6).

DNA-seq was performed as previously described (Shain et al., 2015a). Briefly, 20–250 ng of genomic DNA was prepared for sequencing using the KAPA Hyper Prep Kit (Cat# KK8504). Target enrichment with customized baits (Table S1) was performed using SeqCap EZdeveloper library (Ref #: 06471706001). Sequencing was performed on an Illumina HiSeq 2500 instrument. Alignment, grooming, mutation calling, and copy number calling were performed with the following software packages: Burrows-Wheeler Aligner (BWA) (Li and Durbin, 2009), Genome Analysis Tool-Kit (GATK) (DePristo et al., 2011), Picard (https://broadinstitute.github.io/picard/), MuTect, and CNVkit (Talevich et al., 2016).

Estimation of Tumor Cell Content—Tumor purity was calculated bioinformatically for each sample. When possible, multiple bioinformatic approaches were used. The specific approaches utilized to make this calculation for each sample are iterated in the “Estimation of Tumor Cell Content – Orthogonal Methods” column of Table S2, and detailed descriptions of each approach are as follows:

Germline SNP Del.: Allelic imbalance over germline, heterozygous SNPs is introduced when a heterozygous deletion occurs in a tumor cell. In sequencing reads derived from tumor cells, the percentage of reads mapping to each allele shifts to 100/0, but it remains 50/50 from sequencing reads derived from stromal cells. The extent of allelic imbalance in the overall sampling of reads spanning SNPs on deleted chromosomes is therefore indicative of tumor purity (Shain et al., 2015a). This approach assumes these deletions are fully clonal and heterozygous.

Clustered Heterozygous Mutations: Somatic mutations can be stratified by their mutant allele frequencies (MAFs), which are dictated by the clonality and the zygosity of the mutation. Here, we used the median MAF of somatic mutations occupying portions of the genome without copy number alterations to infer tumor purity. This approach assumes those mutations are fully clonal and heterozygous.

Driver Mutation: Some samples had few mutations, precluding the ‘clustered heterozygous mutation’ method of inference described above, but every sample had at least one driver mutation. The mutant allele frequency of the driver mutation was used to estimate tumor purity under the assumption that the mutation was heterozygous and fully clonal – before making these assumptions, we checked for loss-of-heterozygosity or a copy number alteration affecting the locus of the driver mutation.

Hemizygous Somatic Mutations: Some somatic mutations sometimes occurred on hemizygous chromosomes, meaning there was a deletion of the other allele. The mutant allele frequency of sequencing reads derived from tumor cells should be 100%, whereas sequencing reads from stromal cells do not contribute any mutant reads. The observed mutant allele frequency of the somatic mutation can therefore be used to infer the relative

proportions of tumor and stromal cells (Shain et al., 2015a). This approach assumes these mutations are fully clonal.

Somatically Gained Mutations: Some somatic mutations occurred on chromosomes with a gain, meaning that there two mutant alleles and one non-mutant allele in each tumor cell. The mutant allele frequency of sequencing reads derived from tumor cells should be 66%, whereas sequencing reads from stromal cells do not contribute any mutant reads. The observed mutant allele frequency of the mutation can therefore be used to infer the relative proportions of tumor and stromal cells (Shain et al., 2015a). This approach assumes these mutations are fully clonal and there are 2 mutant alleles along with one wild-type allele in the tumor cells.

X-Chr. Mutations: In a male sample, a somatic mutation on the X chromosome will have a mutant allele frequency 100% from sequencing reads derived from the tumor cells. Sequencing reads from stromal cells will not contribute any mutant reads. The observed mutant allele frequency of the mutation can therefore be used to infer the relative proportions of tumor and stromal cells (Shain et al., 2015a). This approach assumes these mutations are fully clonal.

Germline CNN LOH: Allelic imbalance over germline, heterozygous SNPs is introduced when copy-number-neutral (CNN) loss-of-heterozygosity (LOH) occurs in a tumor cell. In sequencing reads derived from tumor cells, the percentage of reads mapping to each allele shifts to 100/0, but it remains 50/50 from sequencing reads derived from stromal cells. The extent of allelic imbalance in the overall sampling of reads is therefore indicative of tumor purity (Shain et al., 2015a). This approach assumes the LOH is fully clonal.

Construction of Phylogenetic Trees—Copy number segments are included in Table S4, and point mutation calls are included in Table S5. A point mutation or a copy number alteration was counted as present in a sample (for the purposes of constructing a phylogenetic tree) only if they were more than 50% clonal. The expected mutant allelic frequency of a point mutation and the expected amplitude of a copy number amplitude was calculated for each sample after accounting for tumor purity. Clonality of a somatic alteration was determined by its mutant allele frequency (for point mutations) or amplitude (for copy number alterations) relative to this expected value. This cutoff ensured that somatic alterations, which are most likely subclonal or possibly arose from low-levels of cross contamination during microdissection, were not treated as shared, or truncal, events. After designating each somatic alteration as being ‘present’ or ‘absent’ in a sample, phylogenetic trees for individual progression cases were constructed from the shared (trunk) and private (branch) mutations.

RNA-seq and Analysis—One hundred nanograms of total RNA was prepared for sequencing using the KAPA stranded RNA-seq Library Preparation Kit (KR0934). This kit utilizes random priming for cDNA synthesis, resulting in preparation of both messenger RNA and ribosomal RNA. To enrich for mRNAs, target enrichment was performed using xGen Lockdown Reagents from Integrated DNA Technologies (IDT, Cat# 1072281) designed to capture the entire exome (Table S1). 100 bp, paired-end sequencing was

performed on an Illumina HiSeq 2500 instrument. Sequencing reads were aligned using STAR (Dobin et al., 2013), producing both genome and transcriptome alignments. Due to the low library complexity of each sample (discussed above) deduplicated alignments were also produced. Expected read counts were estimated for each gene and isoform from the deduplicated transcriptome alignments using RSEM (Li and Dewey, 2011). Expected read counts were normalized within each sample following the approach set forth by the cancer genome atlas RNA-seq Version 2 pipeline. The proportion of expressed mutant reads was determined using the Samtools mpileup function on the RNA-seq alignments to the genome.

Gene Expression Clustering—For clustering, sample-adjusted RSEM gene-counts were median centered across genes and converted to log scale. We performed centroid-linkage clustering on genes filtered to include those with detectable expression in more than 80% of samples and a minimal standard deviation of expression variability across samples of 1. We attempted several iterations of clustering, using different linkage methods and filtering criteria without observing any meaningful changes in the resulting clusters – samples and genes clustered reproducibly by stage (benign vs malignant) and into a small number of biologically coordinated gene expression programs (as shown in Figure S5). Biologically coordinated gene expression programs were determined by performing Gene Set Enrichment analysis against all signatures from the molecular signature database (http://software.broadinstitute.org/gsea/msigdb).

DATA AND SOFTWARE AVAILABILITY

Genomic Data—Raw sequencing data is available through dbGaP (phs001550.v1.p1).

Mendeley Dataset—The detailed evolution of each case can be downloaded from the Mendeley Dataset, accessible through the following link: https://doi.org/10.17632/nrywwbx6fm.2. This dataset also includes large supplementary tables with bait intervals, mutation calls, copy number segments, and other information associated with each sample in the study.

Supplementary Material

Refer to Web version on PubMed Central for supplementary material.

ACKNOWLEDGMENTS

A.H.S. is supported by the NIH (K22 CA17997, T32 CA177555), the PhRMA Foundation, the Dermatology Foundation, the Melanoma Research Foundation, and the Program in Breakthrough Biomedical Research at UCSF. B.C.B. is supported by an Outstanding Investigatory Award (1R35CA220481) from the NCI, an Individual Investigator Award of the Melanoma Research Alliance, and the Terry Patters Memorial Foundation.

REFERENCES

Balch CM, Gershenwald JE, Soong S-J, Thompson JF, Atkins MB, Byrd DR, Buzaid AC, Cochran AJ, Coit DG, Ding S, et al. (2009). Final version of 2009 AJCC melanoma staging and classification. J. Clin. Oncol 27, 6199–6206. [PubMed: 19917835]

Botton T, Yeh I, Nelson T, Vemula SS, Sparatta A, Garrido MC, Allegra M, Rocchi S, Bahadoran P, McCalmont TH, et al. (2013). Recurrent BRAF kinase fusions in melanocytic tumors offer an opportunity for targeted therapy. Pigment Cell Melanoma Res. 26, 845–851. [PubMed: 23890088]

Cancer Genome Atlas Network (2015). Genomic classification of cutaneous melanoma. Cell 161, 1681–1696. [PubMed: 26091043]

DePristo MA, Banks E, Poplin R, Garimella KV, Maguire JR, Hartl C, Philippakis AA, del Angel G, Rivas MA, Hanna M, et al. (2011). A framework for variation discovery and genotyping using next-generation DNA sequencing data. Nat. Genet 43, 491–498. [PubMed: 21478889]

Ding L, Kim M, Kanchi KL, Dees ND, Lu C, Griffith M, Fenstermacher D, Sung H, Miller CA, Goetz B, et al. (2014). Clonal architectures and driver mutations in metastatic melanomas. PLoS One 9, e111153. [PubMed: 25393105]

Dobin A, Davis CA, Schlesinger F, Drenkow J, Zaleski C, Jha S, Batut P, Chaisson M, and Gingeras TR (2013). STAR: ultrafast universal RNA-seq aligner. Bioinformatics 29, 15–21. [PubMed: 23104886]

Gartner JJ, Davis S, Wei X, Lin JC, Trivedi NS, Teer JK, NISC Comparative Sequencing Program, Meltzer PS, Rosenberg SA, and Samuels Y (2012). Comparative exome sequencing of metastatic lesions provides insights into the mutational progression of melanoma. BMC Genomics 13, 505. [PubMed: 23006843]

Hedegaard J, Thorsen K, Lund MK, Hein A-MK, Hamilton-Dutoit SJ, Vang S, Nordentoft I, Birkenkamp-Demtröder K, Kruhøffer M, Hager H, et al. (2014). Next-generation sequencing of RNA and DNA isolated from paired fresh-frozen and formalin-fixed paraffin-embedded samples of human cancer and normal tissue. PLoS One 9, e98187. [PubMed: 24878701]

Hodis E, Watson IR, Kryukov GV, Arold ST, Imielinski M, Theurillat J-P, Nickerson E, Auclair D, Li L, Place C, et al. (2012). A landscape of driver mutations in melanoma. Cell 150, 251–263. [PubMed: 22817889]

Houben R, Vetter-Kauczok CS, Ortmann S, Rapp UR, Broecker EB, and Becker JC (2008). Phospho-ERK staining is a poor indicator of the mutational status of BRAF and NRAS in human melanoma. J. Invest. Dermatol 128, 2003–2012. [PubMed: 18323787]

Joseph EW, Pratilas CA, Poulikakos PI, Tadi M, Wang W, Taylor BS, Halilovic E, Persaud Y, Xing F, Viale A, et al. (2010). The RAF inhibitor PLX4032 inhibits ERK signaling and tumor cell proliferation in a V600E BRAF-selective manner. Proc. Natl. Acad. Sci. USA 107, 14903–14908. [PubMed: 20668238]

Kerick M, Isau M, Timmermann B, Sültmann H, Herwig R, Krobitsch S, Schaefer G, Verdorfer I, Bartsch G, Klocker H, et al. (2011). Targeted high throughput sequencing in clinical cancer settings: formaldehyde fixed-paraffin embedded (FFPE) tumor tissues, input amount and tumor heterogeneity. BMC Med. Genomics 4, 68. [PubMed: 21958464]

Kleihues P, Schäuble B, zur Hausen A, Estéve J, and Ohgaki H (1997). Tumors associated with p53 germline mutations: a synopsis of 91 families. Am. J. Pathol 150, 1–13. [PubMed: 9006316]

Krauthammer M, Kong Y, Ha BH, Evans P, Bacchiocchi A, McCusker JP, Cheng E, Davis MJ, Goh G, Choi M, et al. (2012). Exome sequencing identifies recurrent somatic RAC1 mutations in melanoma. Nat. Genet 44, 1006–1014. [PubMed: 22842228]

Krauthammer M, Kong Y, Bacchiocchi A, Evans P, Pornputtapong N, Wu C, McCusker JP, Ma S, Cheng E, Straub R, et al. (2015). Exome sequencing identifies recurrent mutations in NF1 and RASopathy genes in sun-exposed melanomas. Nat. Genet 47, 996–1002. [PubMed: 26214590]

Li B, and Dewey CN (2011). RSEM: accurate transcript quantification from RNA-Seq data with or without a reference genome. BMC Bioinformatics 12, 323. [PubMed: 21816040]

Li H, and Durbin R (2009). Fast and accurate short read alignment with Burrows-Wheeler transform. Bioinformatics 25, 1754–1760. [PubMed: 19451168]

Maldonado JL, Fridlyand J, Patel H, Jain AN, Busam K, Kageshita T, Ono T, Albertson DG, Pinkel D, and Bastian BC (2003). Determinants of BRAF mutations in primary melanomas. J. Natl. Cancer Inst 95, 1878–1890. [PubMed: 14679157]

Monsel G, Ortonne N, Bagot M, Bensussan A, and Dumaz N (2010). c-Kit mutants require hypoxia-inducible factor 1alpha to transform melanocytes. Oncogene 29, 227–236. [PubMed: 19802003]

Nikolaev SI, Rimoldi D, Iseli C, Valsesia A, Robyr D, Gehrig C, Harshman K, Guipponi M, Bukach O, Zoete V, et al. (2012). Exome sequencing identifies recurrent somatic MAP2K1 and MAP2K2 mutations in melanoma. Nat. Genet 44, 133–139.

Palescandolo E, Jones R, Raza A, Sunkavalli A, Brastianos PK, Ducar M, Go C, Roden C, Hatton C, Hanna M, et al. (2012). Abstract 3178: can DNA from archived formalin-fixed paraffin embedded (FFPE) cancer tissues be used for somatic mutation analysis in next generation sequencing. Cancer Res. 72, 3178.

Sanborn JZ, Chung J, Purdom E, Wang NJ, Kakavand H, Wilmott JS, Butler T, Thompson JF, Mann GJ, Haydu LE, et al. (2015). Phylogenetic analyses of melanoma reveal complex patterns of metastatic dissemination. Proc. Natl. Acad. Sci. USA 112, 10995–11000. [PubMed: 26286987]

Shain AH, and Bastian BC (2016). From melanocytes to melanomas. Nat. Rev. Cancer 16, 345–358. [PubMed: 27125352]

Shain AH, and Pollack JR (2013). The spectrum of SWI/SNF mutations, ubiquitous in human cancers. PLoS One 8, e55119. [PubMed: 23355908]

Shain AH, Yeh I, Kovalyshyn I, Sriharan A, Talevich E, Gagnon A, Dummer R, North J, Pincus L, Ruben B, et al. (2015a). The genetic evolution of melanoma from precursor lesions. N. Engl. J. Med 373, 1926–1936. [PubMed: 26559571]

Shain AH, Garrido M, Botton T, Talevich E, Yeh I, Sanborn JZ, Chung J, Wang NJ, Kakavand H, Mann GJ, et al. (2015b). Exome sequencing of desmoplastic melanoma identifies recurrent NFKBIE promoter mutations and diverse activating mutations in the MAPK pathway. Nat. Genet 47, 1194–1199. [PubMed: 26343386]

Sharpless E, and Chin L (2003). The INK4a/ARF locus and melanoma. Oncogene 22, 3092–3098. [PubMed: 12789286]

Shi H, Hugo W, Kong X, Hong A, Koya RC, Moriceau G, Chodon T, Guo R, Johnson DB, Dahlman KB, et al. (2014). Acquired resistance and clonal evolution in melanoma during BRAF inhibitor therapy. Cancer Discov. 4, 80–93. [PubMed: 24265155]

Talevich E, Shain AH, Botton T, and Bastian BC (2016). CNVkit: genome-wide copy number detection and visualization from targeted DNA sequencing. PLoS Comput. Biol 12, e1004873. [PubMed: 27100738]

Tan M-H, Mester JL, Ngeow J, Rybicki LA, Orloff MS, and Eng C (2012). Lifetime cancer risks in individuals with germline PTEN mutations. Clin. Cancer Res 18, 400–407. [PubMed: 22252256]

Van Raamsdonk CD, Griewank KG, Crosby MB, Garrido MC, Vemula S, Wiesner T, Obenauf AC, Wackernagel W, Green G, Bouvier N, et al. (2010). Mutations in GNA11 in uveal melanoma. N. Engl. J. Med 363, 2191–2199. [PubMed: 21083380]

Wan PT, Garnett MJ, Roe SM, Lee S, Niculescu-Duvaz D, Good VM, Project CG, Jones CM, Marshall CJ, Springer CJ, et al. (2004). Mechanism of activation of the RAF-ERK signaling pathway by oncogenic mutations of B-RAF. Cell 116, 855–867. [PubMed: 15035987]

Wilson BG, Wang X, Shen X, McKenna ES, Lemieux ME, Cho Y-J, Koellhoffer EC, Pomeroy SL, Orkin SH, and Roberts CWM (2010). Epigenetic antagonism between polycomb and SWI/SNF complexes during oncogenic transformation. Cancer Cell 18, 316–328. [PubMed: 20951942]

Zeng H, Jorapur A, Shain AH, Lang UE, Torres R, Zhang Y, McNeal AS, Botton T, Lin J, Donne M, et al. (2018). Bi-allelic loss of CDKN2A initiates melanoma invasion via BRN2 activation. Cancer Cell 34, this issue, 56–68. [PubMed: 29990501]

Zingg D, Debbache J, Schaefer SM, Tuncer E, Frommel SC, Cheng P, Arenas-Ramirez N, Haeusel J, Zhang Y, Bonalli M, et al. (2015). The epigenetic modifier EZH2 controls melanoma growth and metastasis through silencing of distinct tumour suppressors. Nat. Commun 6, 6051. [PubMed: 25609585]

Zingg D, Arenas-Ramirez N, Sahin D, Rosalia RA, Antunes AT, Haeusel J, Sommer L, and Boyman O (2017). The histone methyltransferase Ezh2 controls mechanisms of adaptive resistance to tumor immunotherapy. Cell Rep. 20, 854–867. [PubMed: 28746871]

Highlights

- Evolution of melanoma from precursors revealed through sequencing of DNA and RNA
- MAPK pathway output progressively ramps up during progression
- The chromatin landscape is reconfigured at the transition to melanoma
- G1/S checkpoint override coincides with transition from *in situ* to invasive melanoma

Significance

This study further delineates the sequential order in which signaling pathways become disrupted as benign and intermediate precursors evolve to melanoma in situ, invasive melanoma, and metastases. Activation of the MAPK pathway induces a benign nevus, constrained by replicative senescence, G1/S arrest, and chromatin organization. These barriers are incrementally overrun during melanoma formation, and melanomas continue to accumulate genetic alterations that ramp-up MAPK pathway signaling output and perturb the p53 and PI3K pathways. No mutations were specifically associated with metastatic dissemination to regional sites. Overall, we identify crucial steps in the development of melanoma, which can be subject to future treatments and can guide biomarker strategies to improve diagnosis and staging.

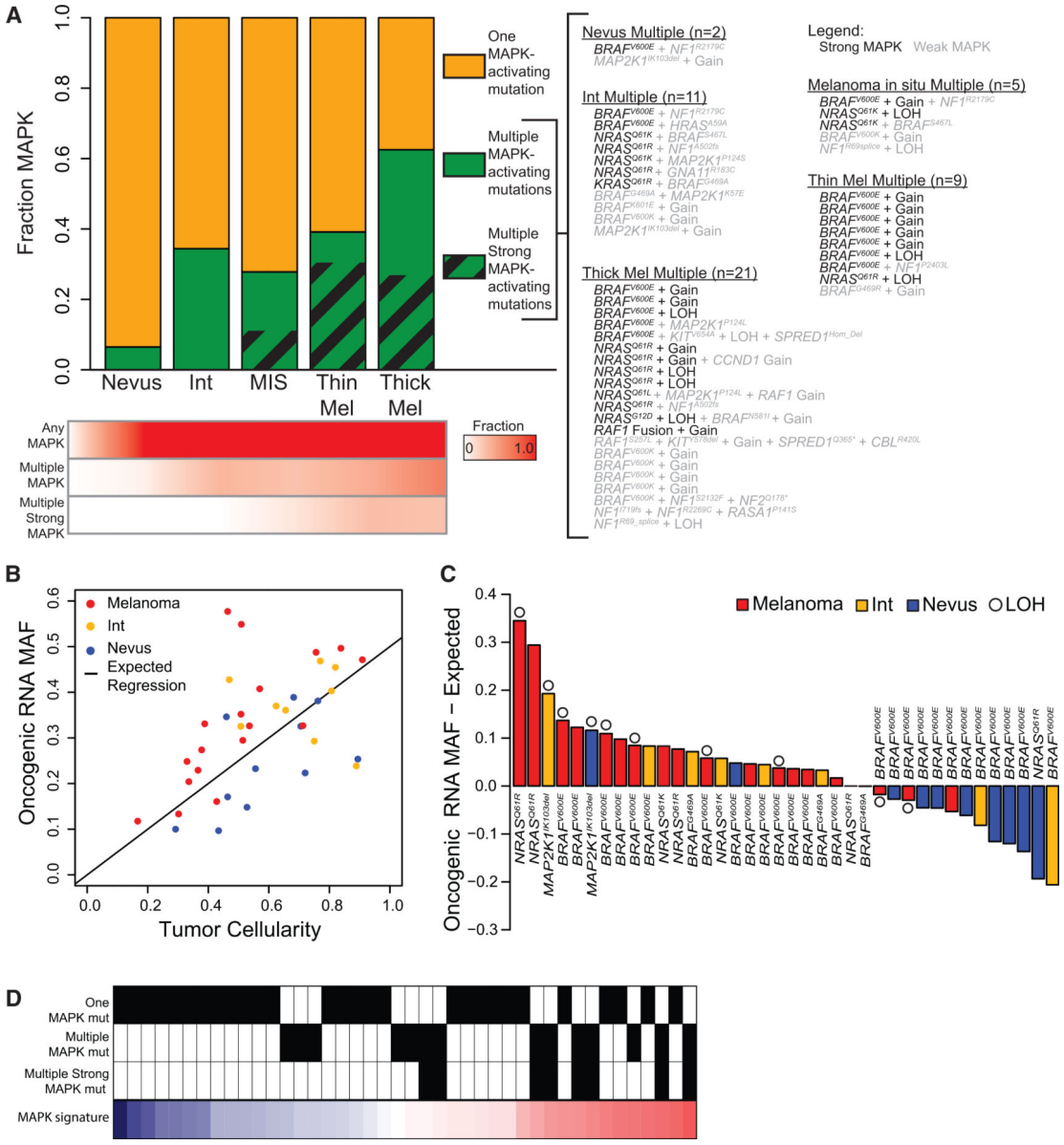

Figure 1. Genetic and Transcriptomic Data Implicate Activation of MAPK Signaling at Initiation and Subsequent Amplification of Signaling during Melanoma Progression

For a Figure360 author presentation of Figure 1, see http//dx.doi:10.1016/j.ccell.2018.06.005#mmc7.

(A) The fraction of mutations (y axis) predicted to activate the MAPK signaling pathway at each stage of melanoma progression. The green bars denote multiple mutations in the same sample with the specific combinations iterated to the right. Strong and weak activators of MAPK signaling are separately annotated (see the STAR Methods for details on classifying strong and weak mutations).

(B) The mutant allele fraction (MAF) of oncogenic MAPK mutations from RNA-seq data is plotted as a function of tumor purity (cellularity). The regression line indicates the expected relationship under a model in which the transcript level from the mutant allele is proportional to tumor purity.

(C) Proportions of oncogenic transcript after accounting for tumor cell content (melanoma versus nevus, $p = 10^3$, t test). The specific driver mutations and their allelic status (loss-of-heterozygosity [LOH] or not) are also annotated for each neoplasm.
(D) MAPK signaling output was inferred from an established MAPK gene expression signature (Joseph et al., 2010). Red and blue bars, respectively, denote a relatively more/less intense signature. The number of mutations in the MAPK pathway are indicated for each sample.See also Figure S2 and Table S3.

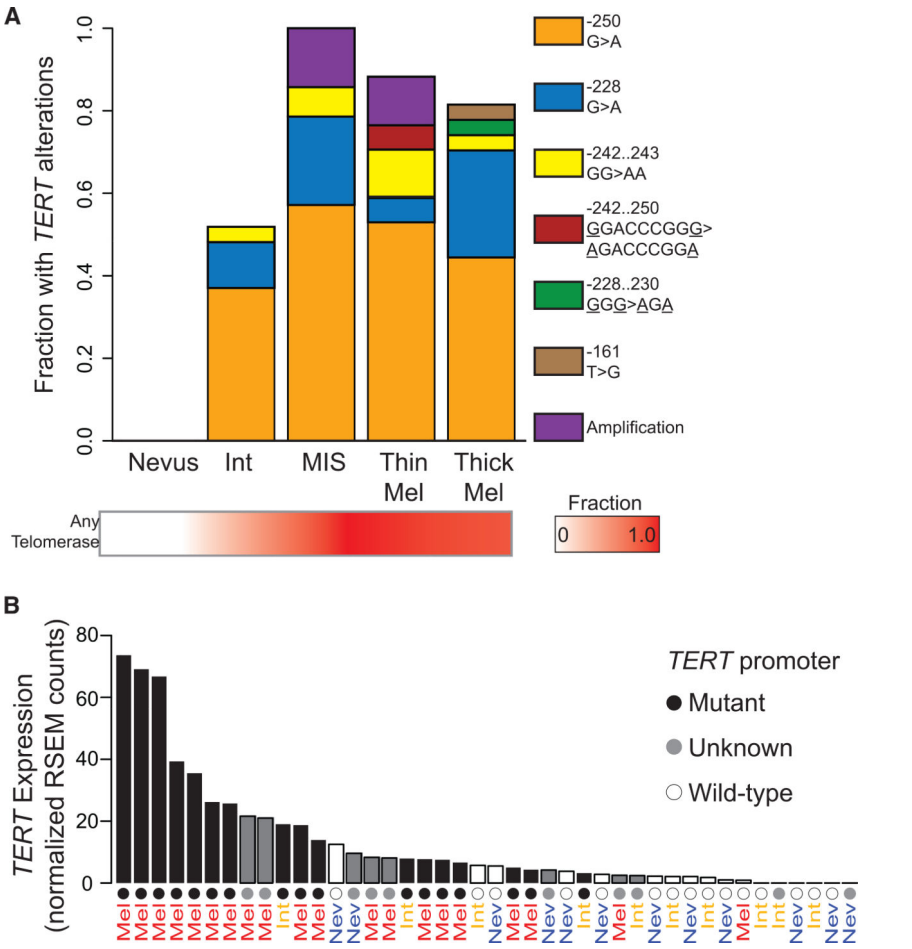

Figure 2. Genetic and Transcriptomic Data Implicate Upregulation of Telomerase Early during Melanoma Progression

(A) The fraction of genetic alterations (y axis) affecting *TERT* at each phase of melanoma progression.

(B) *TERT* expression was inferred from RNA-seq data and plotted from highest to lowest (left to right) with stage and mutation status designated. p values were calculated by comparing *TERT* expression between groups with two-tailed t tests: melanoma versus nevus, $p = 6.7 \times 10^{3}$; mutant versus wild-type, $p = 10^{3}$.

See also Figure S3.

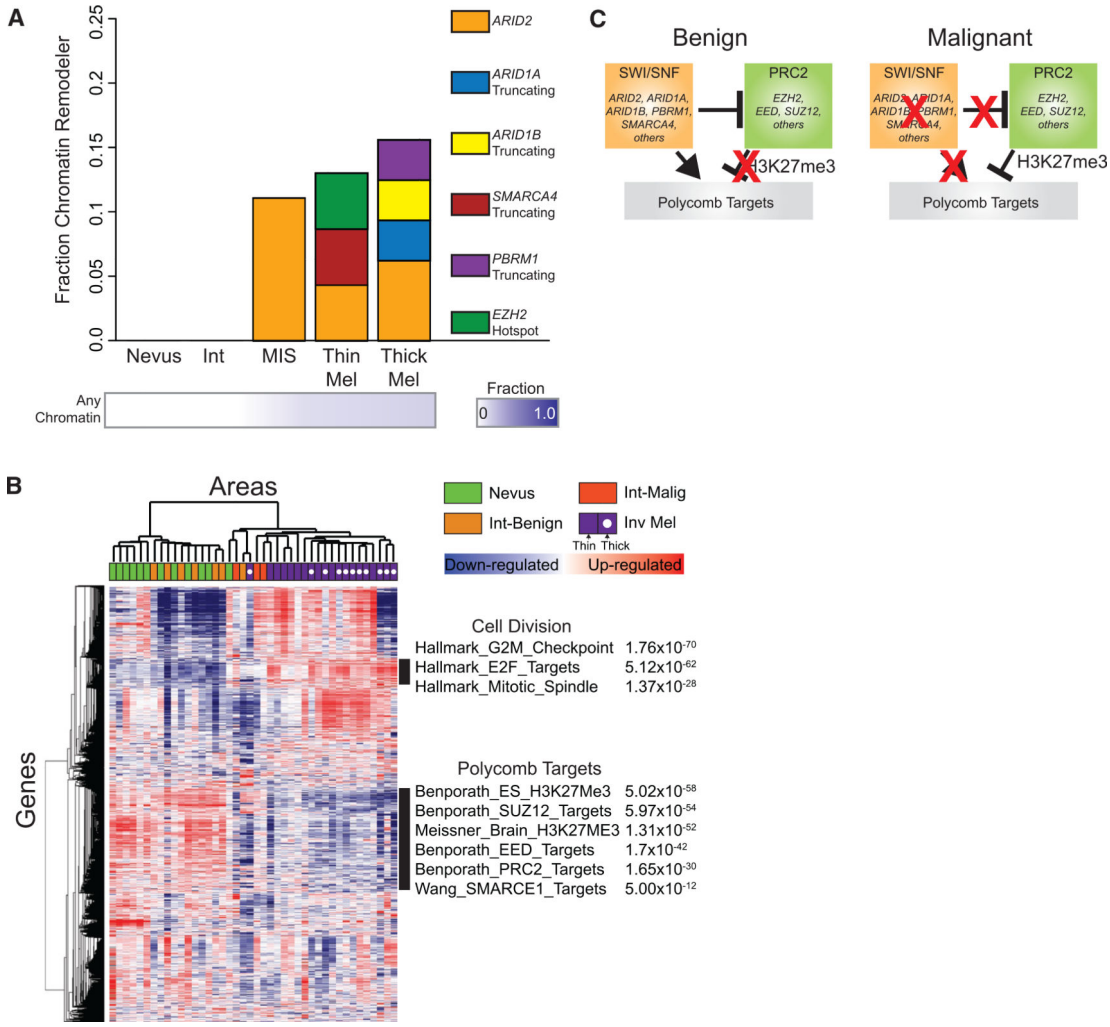

Figure 3. Genetic and Transcriptomic Data Indicate a Shift toward a PRC2-Modulated Chromatin Landscape at the Transition to Melanoma

(A) The fraction of pathogenic mutations in components of the SWI/SNF and PRC2 chromatin remodeling complexes (y axis) at each phase of melanoma progression. To avoid obscuring our analysis with passenger mutations, we only considered bona fide pathogenic alterations (see the STAR Methods).

(B) Unsupervised clustering of samples (columns) and genes (rows) from RNA-seq data. The progression phase of each area and relative expression level of each gene are indicated. Two gene expression clusters are highlighted here (black bars). Gene sets significantly overlapping with the highlighted gene clusters are annotated alongside their q values (see the STAR Methods).

(C) A model summarizing the balance between SWI/SNF and PRC2 during melanoma evolution.

See also Figures S4 and S5.

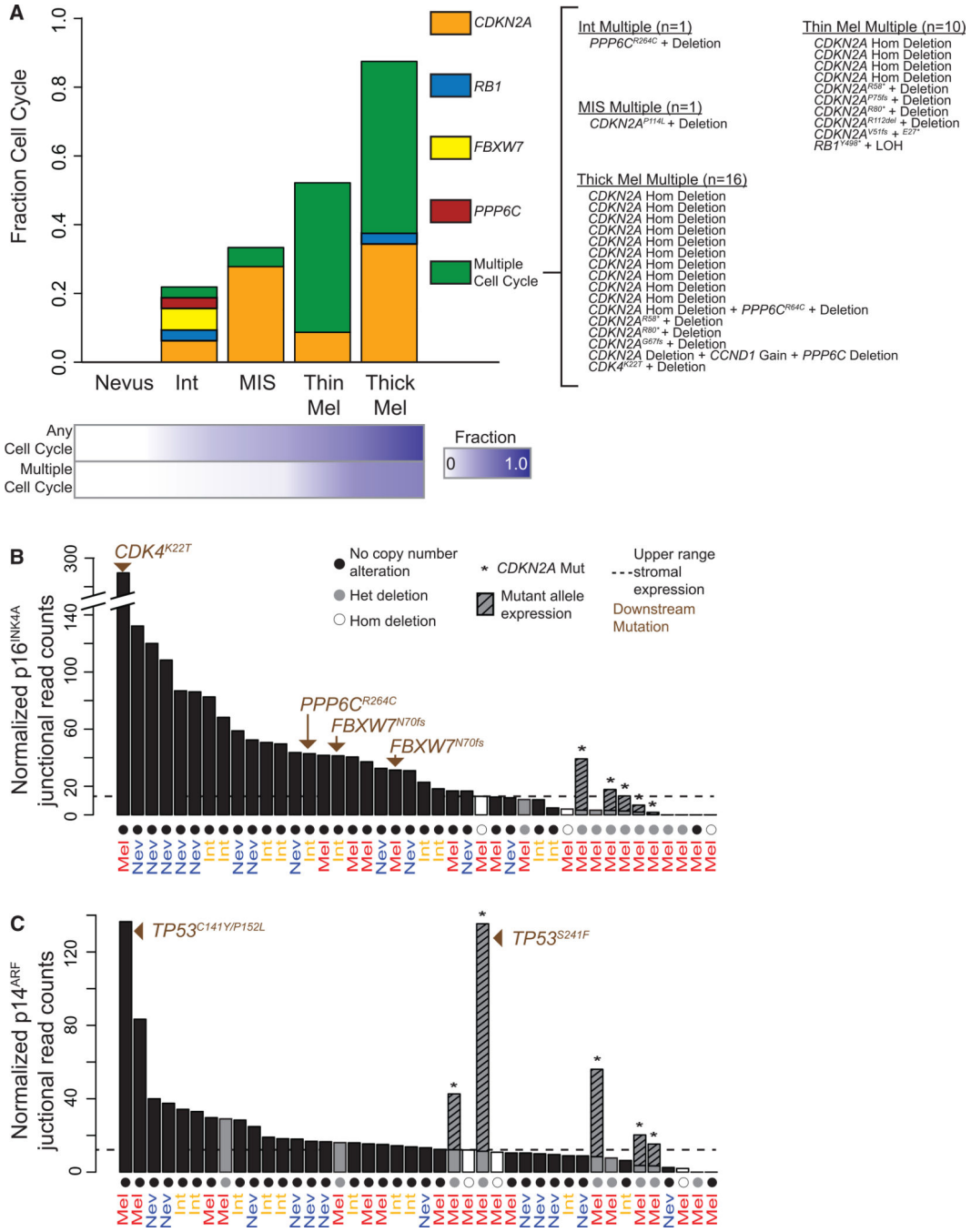

Figure 4. Genetic and Transcriptomic Data Implicates Impairment of the G1/S Checkpoint at the Transition to Invasive Melanoma

(A) The fraction of genetic alterations affecting genes involved in cell-cycle regulation (y axis) at each phase of melanoma progression. The green bars denote multiple mutations in the same sample with the specific combinations iterated to the right.

(B and C) $p16^{INK4A}$ (B) and $p14^{ARF}$ (C) expression levels were inferred from junctional read counts specific to each transcript and are rank ordered from highest to lowest (left to right). The stage of each neoplasm is indicated (x axis) along with the mutation status of $p16^{INK4A}$ or $p14^{ARF}$. The upper range of stromal expression (dotted line) was inferred from

expression in tumors with loss of both alleles, a scenario in which all wild-type expression must derive from stromal cells. The asterisk (*) denotes samples with a point mutation in the *CDKN2A*, and proportion of mutant transcript is indicated by the striped bars.
See also Figure S6.

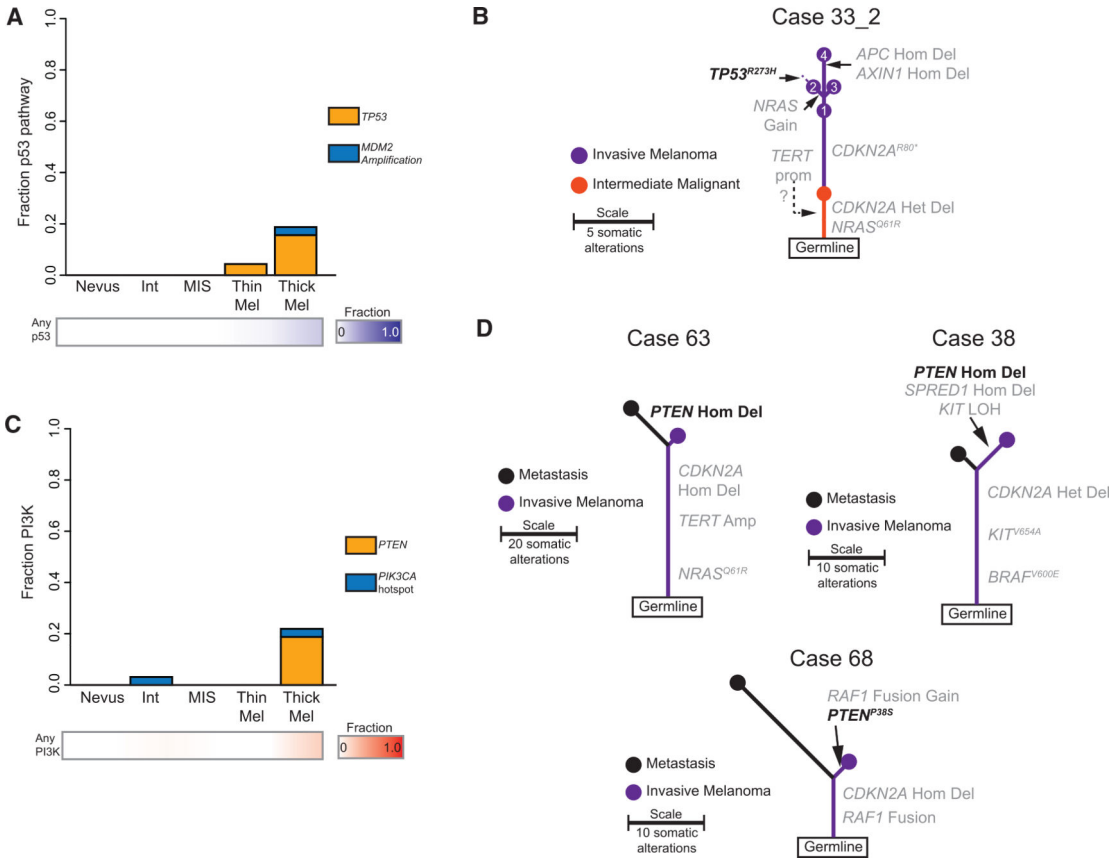

Figure 5. p53 and PI3K Pathway Mutations Appear Comparatively Later during the Evolution of Melanoma

(A) The fraction of genetic alterations affecting genes involved in the p53 pathway (y axis) at each phase of melanoma progression.

(B) Phylogenetic tree for a select *TP53*-mutant case—the detailed evolution of this case is shown in the affiliated Mendeley Dataset. Pathogenic mutations are annotated with the *TP53* mutation highlighted in bold.

(C) The fraction of genetic alterations affecting genes involved in the PI3K pathway (y axis) at each phase of melanoma progression.

(D) Phylogenetic trees for select *PTEN*-mutant cases—the detailed evolutions of these cases are shown in the affiliated Mendeley Dataset. Pathogenic mutations are annotated with the *PTEN* mutations highlighted in bold.

See also Figure S7.

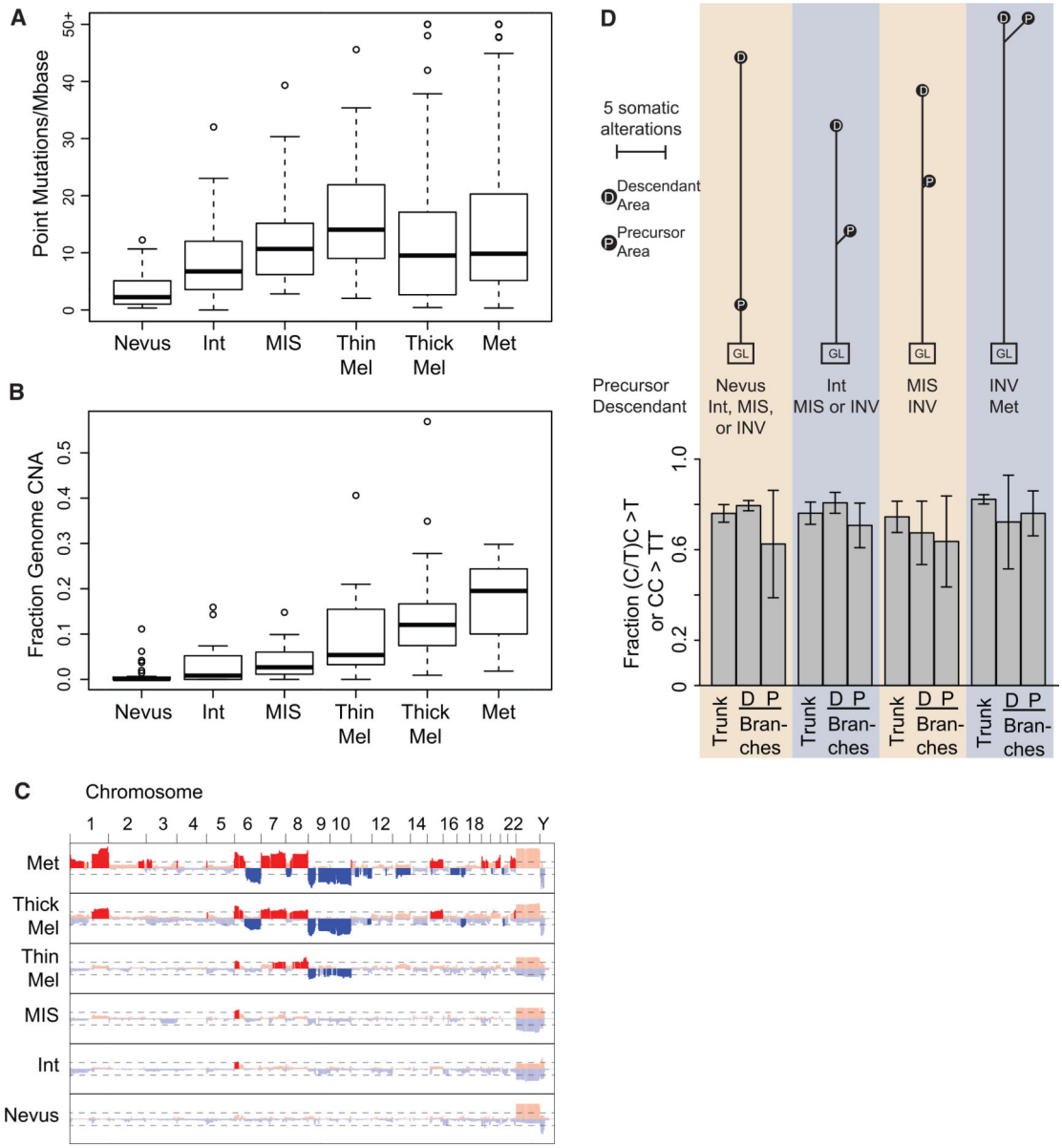

Figure 6. Distinct Mutational Signatures Are Apparent at Specific Evolutionary Time Points

(A–C) The point mutation (A) and copy-number (B) burden at each phase of melanoma progression. Line, median; box, interquartile range (25%–75%); whiskers, 2 SDs above and below the median of the data; circles, outlier data points (C). The copy-number landscape at each phase of progression. Copy-number alterations reaching and remaining above a frequency of 10% are highlighted: red, gain; blue, loss.

(D) Canonical phylogenetic trees corresponding to the four main progression trajectories constructed from the median trunk and branch lengths of all the individual cases (upper). The fraction of UV radiation-induced mutations within the trunks and branches of each progression trajectory (lower): D, descendant;P, precursor, mean ± 95% confidence intervals are shown.

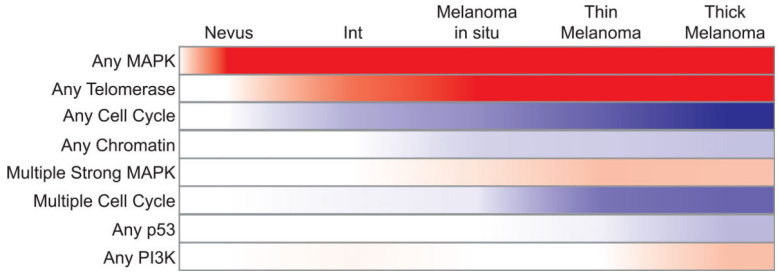

Figure 7. Somatic Alterations in Key Signaling Pathways that Drive Melanoma Appear at Specific Points in the Melanoma Progression Cascade

Each heatmap reflects the frequency that a given pathway is activated (red) or inactivated (blue) at a specific point in the melanoma progression cascade.

KEY RESOURCES TABLE

REAGENT or RESOURCE	SOURCE	IDENTIFIER
Biological Samples		
Archival melanocytic neoplasms	UCSF Dermatopathology Archive	https://dermpath.ucsf.edu/services-overview/
Critical Commercial Assays		
KAPA Hyper Prep Kit	KAPA Biosystems	p/n KK8504
SeqCap EZdeveloper	Nimblegen	p/n 06471706001
Deposited Data		
Raw sequencing data	This paper	dbGaP phs001550.v1.p1
Burrows-Wheeler Aligner (BWA)	Li and Durbin, 2009	http://bio-bwa.sourceforge.net/
Genome-Analysis Toolkit	DePristo et al., 2011	https://software.broadinstitute.org/gatk/
Picard	https://broadinstitute.github.io/picard/	https://broadinstitute.github.io/picard/
MuTect	http://archive.broadinstitute.org/cancer/cga/mutect	http://archive.broadinstitute.org/cancer/cga/mutect
CNVkit	Talevich et al., 2016	https://cnvkit.readthedocs.io/en/stable/
Other		
Case by case analyses	This paper	https://doi.org/10.17632/nrywwbx6fm.2